ELEVON-ELEVON GAP FOW IMPINGEMENT

José M. A. Longo[(1)], Bodo Reimann[(1)], Silvia Strom[(1)], Rolf Radespiel[(2)], Malte Esdorf[(2)], Torsten Wolf[(2)]

[(1)]German Aerospace Center, DLR, Institute of Aerodynamics and Flow Technology,
Lilienthalplatz 7, 38108 Braunschweig, Germany, jose.longo@dlr.de
[(2)]Technische Universität Braunschweig, Institute of Fluid Mechanics,
Bienroder Weg 3, 38106 Braunschweig,Germany, radespiel@tu-bs.de

ABSTRACT

The paper presents an experimental and numerical investigation of the unsteady, transitional flow resulting at a cantilever flap configuration of a space vehicle in cold hypersonics. The goal of the study is to investigate the potential to use an aerodynamic controlled vehicle for an aerobraking manoeuvre when returning from a Moon mission. An experimental investigation is carried out in the high-speed Ludwig tube facility of the Technische Universität Braunschweig, at Mach 6, Reynolds numbers varying from 2.4 10^6 to 1.7 10^7, and supported by numerical solutions obtained with the TAU code of the DLR. The analysis of the experimental and numerical results displays a complex unsteady flow topology at the control surfaces, with severe hot points resulting from shock-shock interaction, shock-boundary layer interaction and jet flow in the gap between the flaps. The resulting jet impingement at the flaps results in heat fluxes which largely surpass the stagnation point heat flux. Such situation becomes more severe as the flow evolves from almost laminar for the low Reynolds number case to transitional at the flaps for the high Reynolds number case. It turns out aerobraking manoeuvres with aerodynamic controlled vehicles should be carefully designed since shock-shock interactions may jeopardizing the whole mission.

1. INTRODUCTION

The DLR Institute of Aerodynamics and Flow Technology has realized a feasibility study for a Moon sample return mission comprising in particular a super orbital Earth re-entry with or w/o aerobraking [1]. The space tug vehicle comprises a lunar polar-orbit satellite for relay communications and potential remote scientific investigations; a Moon lander with a rover for surface automatic research and a lunar ascent stage module for transportation of probes from the Moon surface to a low lunar orbit; finally a return spacecraft for transportation of the probes to Earth designated as RFMEX (Return Flight Moon Experiment). Such re-entry Vehicle will transfer the lunar samples to the Earth demonstrating an gliding atmospheric re-entry at velocities over 11 km/s. Planned is an actively controlled vehicle which may manoeuvre autonomously to improve landed location. Within this goal it is important to qualify previously the flight control system based on aerodynamic surfaces and centre of gravity displacement. Three classes of vehicle have been considered: capsule, lifting body and winged body. The advantage of the capsule concept is that it features a simple design but presents a very low design evolution capability; its gliding capacity is very low; has limited guidance and controlling properties, and the landing dispersion is broad, resulting in larger costs for recovery operations. A winged body presents a considerably higher mass compared to other concept classes and therefore is not a feasible concept for a Moon mission. Also the protection of the wings from the resulting re-entry heating due to a direct re-entry with super orbital velocity is a hard problem. Here the lifting body class has been selected as the best option. The selected concept has a good design feasibility, robustness, maturity and growth potential. This selection is fully compatible with extensive national efforts to develop a fully controllable re-entry vehicle, like the German DLR SHEFEX Program [2].

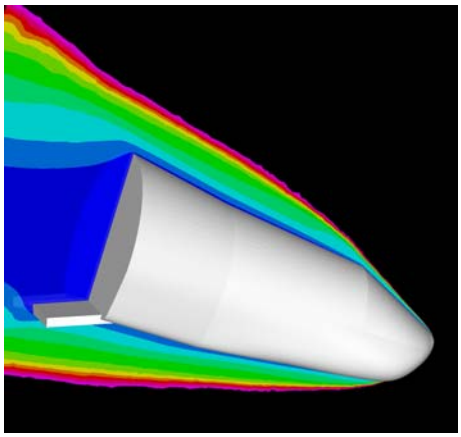

Figure 1: Return Flight Moon Experiment RFMEX

For the present study a lifting body aeroshape having a length of 2.2m, a width of 1.1m and a height of 1m is selected (Fig. 1). The design of the shape ensures maximum volume efficiency due to a limited weight of 460 kg. The interior equipment include the docking system for the lunar samples container; avionics like internal sensors and the telemetry tracking system; Li-Ion battery supply; actuators system for flaps and parachute/safeguard system as well as room for potential passenger experiments; flashing rendezvous

beacon/retractable forward-facing spot lights and airbags for a soft landing. The selected shape exhibits a lift to drag ratio in the range 0.6 to 0.98. Two body flaps, main components of the aerodynamic control system, are located at the rear of the vehicle in a cantilevered configuration. They are used for vehicle trimming and altitude control. Also they can be deflected symmetrically and asymmetrically to assure the flap and aileron control function. At the same time longitudinal and vertical centring is foreseen to assure conditions for longitudinal/ lateral stability. The selected shape is generic and will be optimized within further studies, being the extreme heat loads during re-entry and the stability, controllability and trimmability of the vehicle the primary goals of such activities.

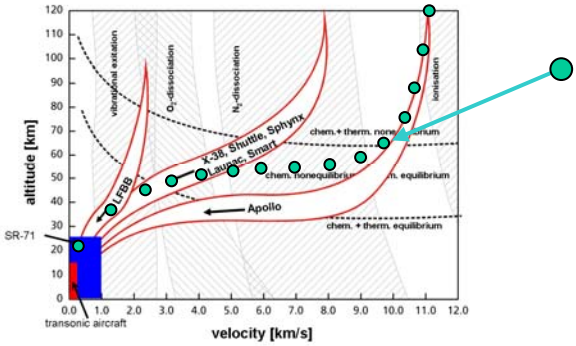

Figure 2: altitude-velocity re-entry diagram. Green dots indicate the RFMEX trajectory.

The aerothermal loads depend onthe re-entry trajectory-profile selected for the mission (Fig. 2). In general it is possible to perform an Earth re-entry from a hyperbolic trajectory directly with super orbital velocity or by previous reduction of the velocity from second to first cosmic velocity by means of an aero-braking manoeuvre. Aerobraking is the term applied to the practice of changing the spacecraft orbit by using the atmospheric drag to reduce the orbit energy in repeated passes. Performing a direct super orbital velocity re-entry with a flight path angle lower than 5deg the heat flux at the stagnation point of the vehicle nose cap is about 14 MW/m^2. Furthermore, the maximal vehicle deceleration may not overshoot the 45g to allow the use of aluminium alloy for the primary structure. Then, in order to relax the re-entry conditions here the potential to perform an aerobraking manoeuvre with an aerodynamic controlled vehicle is investigated. The paper presents the results of the experimental and numerical investigation carried out for a cold hypersonic Mach number M=6 corresponding to a flight altitude of 40km.

2. WIND TUNNEL EXPERIMENTS

2.1. Test facility

The Hypersonic Ludwieg tube Braunschweig (HLB) is a cold blow-down test facility with design Mach number M = 5.9 and unit Reynolds numbers ranging from Re = $2.5 \cdot 10^6$ to $20 \cdot 10^6$. The diameter of the test section is 500mm and the measurement time is about 80ms. The flow conditions are determined from measurements of the initial driver tube pressure and from measurements of the stagnation temperature in the tube during each run. A schematic view of the facility is shown in Fig. 3. Details on the operation of the facility and on the flow conditions including various experimental and numerical results can be found in [3-5]. The free stream conditions are listed in Tab. 1.

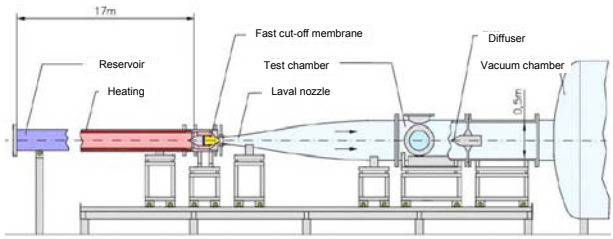

Figure 3: Schematic drawing of the HLB

Table 1. Experimental free stream data.

P_{tube} [bar]	$P_{t\infty}$ [bar]	$T_{t\infty}$ [K]	Ma_∞ [1]	Re_∞/l [10^6/m]
3	2.80±0.05	491±5	5.85±0.03	2.43
8	7.46±0.05	487±5	5.88±0.03	6.54
15	13.99±0.05	485±5	5.91±0.03	12.3
20	18.65±0.05	476±5	5.93±0.03	16.9

2.2. Models

Two wind tunnel models were used for the present study: a hyperboloid / flare geometry as reference data for the selection of the turbulence model to be used in the numerical investigation and the RFMEX geometry. For infrared measurements the models were made from Plexiglas (black 811-Röhm-GS) which is easy to machine and has known thermo-physical properties [5]. The models were coated with Nextel Velvet Coating for high emissivity and low transparency [6]. The thickness of the coating is about 60µm.

2.2.1 Hyperboloid/Flare-model

The hyperboloid / flare model is an axis-symmetric body which is easy to fabricate and at the same time allows for comparing experimental results to 2D computations. The geometrical definition given in [7] represents the contour of the windward side of the Hermes spacecraft at 30° angle of attack including a flap with 20% of the total length and a flap angle of

43.6° related to the axis. The model used for the experiments has a total length of 59.4mm.

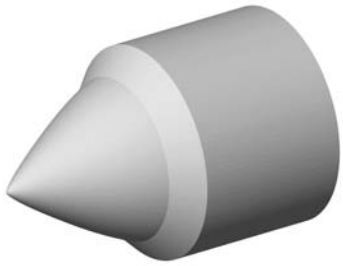

Figure 4: Hyperboloid / flare wind tunnel model

This model was used in the past for validation of infrared measurements and heat-flux evaluation methods by comparing the results to those gained from micro-thermocouple measurements on a thin-walled model with the same geometry [4]. Here the investigation focus on comparing the experimental heat flux to results of simulations with different turbulence models.

2.2.2 Return Flight Moon Experiment RFMEX

The return vehicle RFMEX follows the lifting body concept. The vehicle is controlled by two body flaps. For the presented study only the configuration with 20° flap deflection angle and 45° angle of attack was investigated. The total length of the model is 22cm. A picture of the model is shown in Fig. 5.

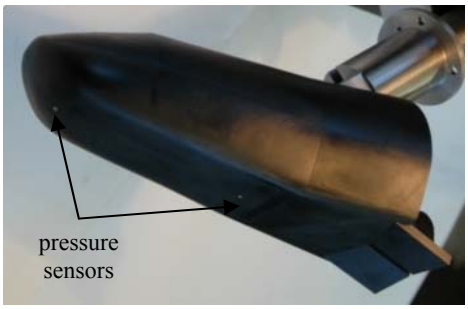

Figure 5: Plexiglas Model without black coating

The model is equipped with two Entran EPIH pressure sensors in the symmetry plane as can be seen in Fig. 5. However, the rear sensor was lost due to particle impact in one of the first experiments. Hence, only measurements from the sensor at the nose could be compared to computational results. During each run a high sped camera was used to record a series of schlieren pictures.

2.3. Heat flux measurements

2.3.1 Infrared camera, temperature calibration

Surface radiance was measured with a "Phoenix DAS" high speed infrared camera system by Indigo Systems. The camera has a 320x256 InSb sensor and measures within the spectral range from 3 to 5µm. The integration time chosen for the measurements was 2ms (2.5ms at smaller pressures) and the frame rate was 230Hz (208Hz) giving about 18 (16) frames per tunnel run. The temperature calibration for each measurement setup was done using a black radiator installed in the measurement section in place of the model. Neither focussing nor positioning of the camera was changed after calibration. A parabolic calibration curve was fitted through 8 to 10 calibration points in the range from 20°C to 60°C. The non-uniformity of the pixel-sensitivities was eliminated first order accurate by two point corrections.

2.3.2 Spatial image calibration

Image coordinates were mapped to space coordinates by using 2D calibration grids. In case of the hyperboloid a curved grid was applied to the surface yielding a calibration accuracy of ±0.3mm in axial direction. Due to a limited field of view of the camera, the measurements on the RFMEX were split into a front and a rear view in different tunnel-runs at similar conditions. For calibration a plane grid was laid accordingly onto the front and rear plane areas of the windward surface yielding only approximate spatial calibrations with estimated uncertainties of ±1mm within the calibrated planes. Note that the use of plane grids implies considerable higher uncertainty on the curved parts of the surface and on the flaps.

2.3.3 Calculation of heat fluxes

1D nonlinear heat conduction perpendicular to the surface is assumed for the calculation of surface heat fluxes from the transient temperature data. For that the conduction into the Plexiglas is modelled by a finite difference method. The surface heat flux is found iteratively by comparing the calculated temperature response to the measured temperatures in a least square formulation, in each interation. The gradient for iterative correction of the heat flux is found by solving the adjoint problem. A regularising criterion adjusted to the noise of the measurements is used for stopping the iteration. Details on the temperature calibration, spatial mapping and the method of heat flux calculation together with an extensive discussion of measurement errors can be found in [4]. There the overall uncertainty of the measured heat fluxes is estimated to be about ±4%.

3. NUMERICAL SIMULATIONS

3.1. DLR TAU code

The flow solver used in the present study is the DLR TAU code [8]. This code is a finite volume Euler/Navier-Stokes solver, which can handle structured, unstructured, and hybrid meshes and has already been applied to a variety of configurations. The Reynolds-averaged Navier-Stokes (RANS) equations are discretized by a finite volume technique using tetrahedrons and prisms. The AUSMDV second-order upwind scheme with MUSCL reconstruction is used for the inviscid fluxes. For time discretization, including local time stepping, a three stage Runge-Kutta, as well as an implicit, approximately factored LU-SGS scheme is implemented. For acceleration, multi-grid and explicit residual smoothing are available. Furthermore, parallel computing is possible via domain splitting and Message Passing Interface (MPI) communication. For hybrid and unstructured grids adaptation by cell division offers the possibility to insert additional points only in regions where clustering is necessary. Based on the flow solution points can be added, redistributed or removed. Figure 6 shows a cut plane of the initial grid around the RFMEX vehicle and the grid after three adaptation steps.

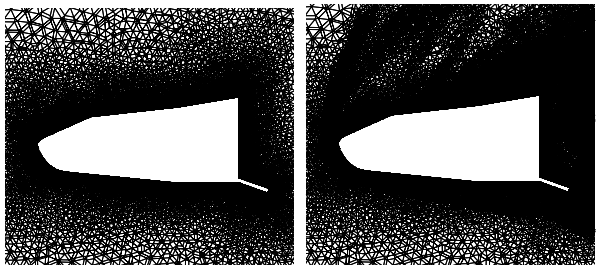

Figure 6: Grid around the RFMEX vehicle. The initial grid is shown on the left-hand side, the adapted grid on the right hand-side.

The transition from laminar to turbulent flow is modelled by prescribing the transition location. In order to model the hypersonic boundary layer flow accurately, an extensive study of turbulence models implemented in the TAU code (2005.1.1) is conducted. The list comprises the one-equation models Spalart-Allmaras (SA), strain-adaptive linear Spalart-Allmaras (SALSA) and Spalart-Allmaras with Edwards modification (SAE) as well as the two-equation models Wilcox k-ω, Menter Baseline, Menter SST, LEA k-ω, Wilcox k-ω with SST modification, NLR TNT and the Menter 2-layer k-ε model.

4. RESULTS

4.1. Hyperboloid/Flare

Heat flux measurements and flow simulations of the laminar flow around the model indicate that for this operating point laminar/turbulent transition occurs across the separation bubble at the hinge. Hence, the production terms in the turbulence models are forced to zero upstream of this location. The resulting Stanton number distributions are compared to thin-film measurements and infrared thermography results.

For the numerical simulation an axis-symmetric computational grid consisting of approx. 300000 grid points and a wedge angle of 3 degrees is used. The y+-value peaks at the model tip (1.1) and end of the flap (0.7) and goes down to 0.1 near the hinge. The inflow boundary conditions are taken from a simulation of the stationary axis-symmetric flow field in the HLB during measurement time and a storage tube pressure of 8.75bar. Depending on the turbulence model the boundary conditions contain distributions for ν_t or k and ω. Convective fluxes are calculated with second-order accurcy using the AUSMPW+ scheme while local-time-stepping is done by means of the implicit LU-SGS algorithm.

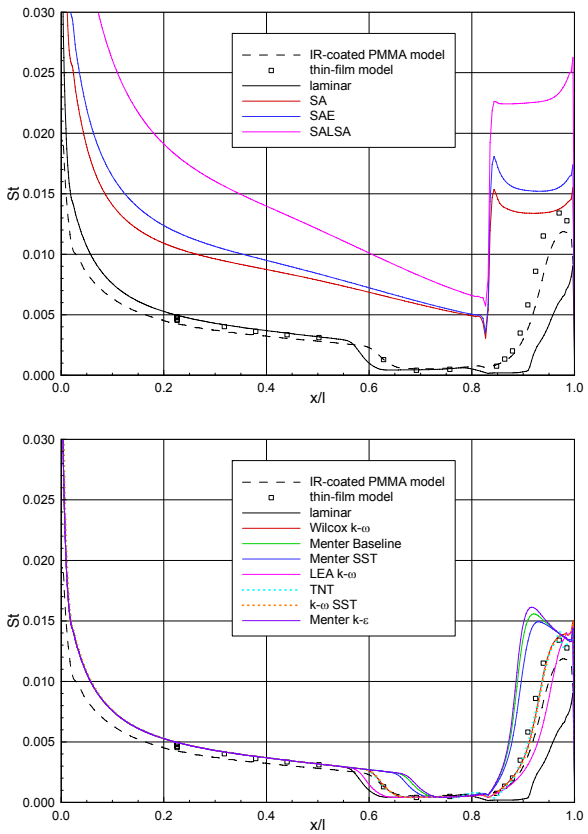

Figure 7: Experimental and numerical Stanton number distributions for the hyperboloid/flare model. Top: 1 equation models. Bottom: 2 equation models.

Figure 7 shows the results for all tested turbulence models. The heat transfer as predicted by all 1-equation models indicates that the flow along the fore body is already turbulent, even though the production terms are disabled until the hinge. Obviously, the convection of incoming turbulence is sufficient to force a turbulent flow along the hyperboloid. Thus, the computed heat transfer is much higher than in the experiments. On the opposite, the 2-equation models maintain a laminar flow until the hinge but yield different separation lenghts. While the LEA k-ω model predicts a large separation zone similar to a fully laminar simulation, the Menter models (Baseline, SST and 2-layer k-ε) lead to a shorter bubble than in the measurements. The most accurate results are obtained with the Wilcox k-ω models and the NLR TNT model. The predicted Stanton number distributions agree very well with the experiments, especially with the thin-film measurements. For the numerical study of the RFMEX configuration the Wilcox is therefore selected.

4.2. Moon return vehicle RFMEX

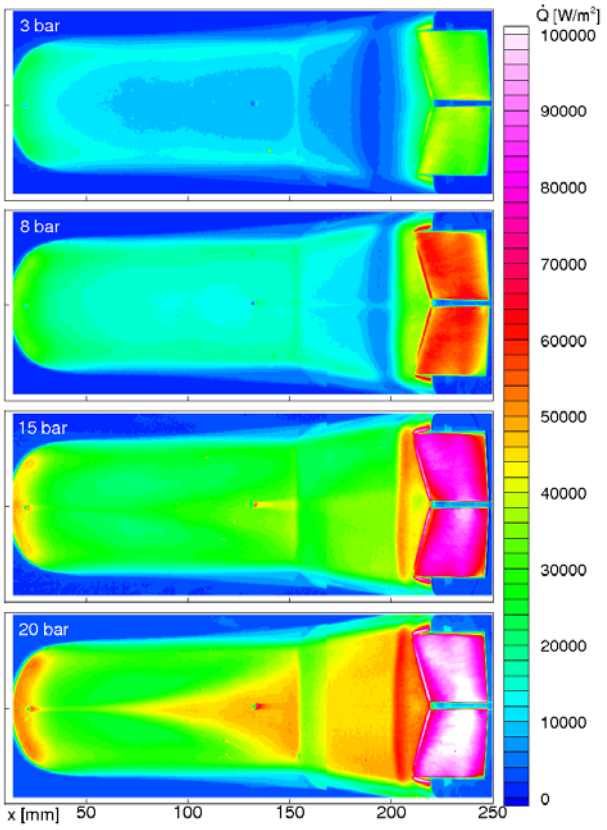

Figure 8: Experimental heat flux densities measured on the wind-ward side of the RFMEX vehicle

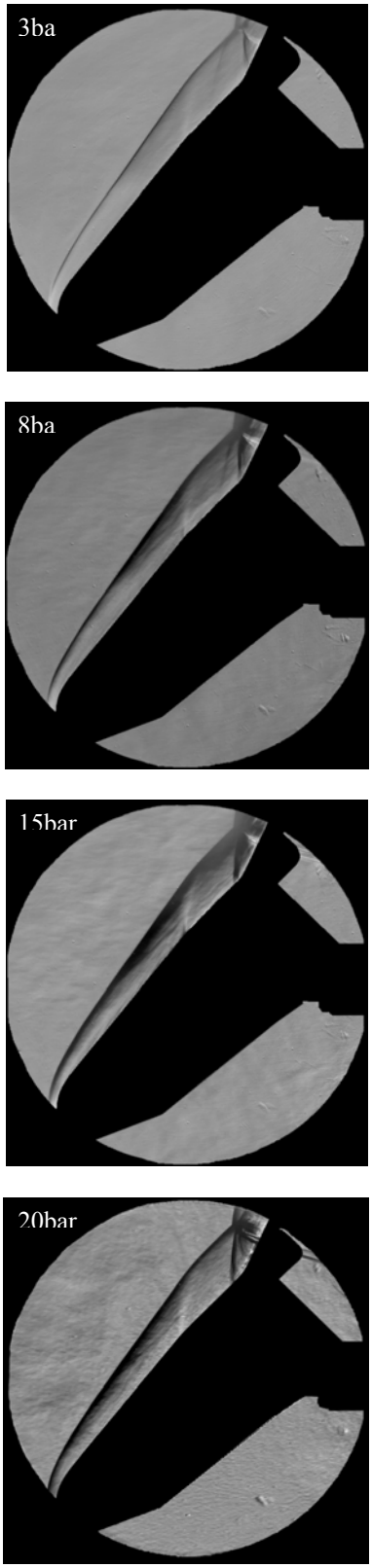

Figure 9: Schlieren pictures of the RFMEX in HLB at condition with 3, 8, 15 and 20bar tube pressure

The measured distributions of the heat flux densities for the RFMEX vehicle at different HLB conditions are shown in Fig. 8. Especially the results for the high Reynolds number conditions (15 and 20bar) show a wedge of increased heat flux behind the positions of the two pressure transducers. The reason is a change of the behaviour of the flow from laminar to turbulent at the pressure port at the wall. Also, for all investigated conditions, the flaps present heat fluxes largely surpassing the stagnation point value and hence indicating a turbulent boundary layer condition at the control surfaces. Figure 9 shows schlieren pictures of the vehicle during the tests. The flow field is dominated by a strong bow shock at the front of the body. The deflection of the control surface leads to control surface shock at the hinge line which due to boundary-layer separation splits into in a separation and attachment shock. The interaction between these shocks and the bow shock results in a complex three- dimensional shock-shock-interaction in the vicinity of the flaps. The time-resolved schlieren image indicates an unsteady characteristics of the flow separation and the shock-shock interaction. A jet flow emerging from the shock-shock interaction and expanding from the windward to the leeward side of the flaps is also visible in the schlieren pictures. As result of jet flow impingement, the flaps present an absolute maximum in heat flux at the inner lateral sides as indicates figure 8.

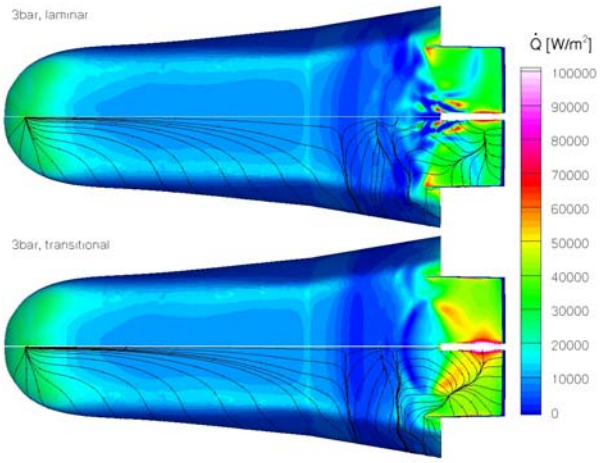

Figure 10: Computed laminar and transitional heat flux density with skin friction lines for RFMEX in HLB 3bar condition

Figures 10 to 12 show numerical results for the 3, 15 and 20bar HLB conditions. The figures show the heat flux density distribution in same scale as that used for the experimental results (figure 8) and skin friction lines. Depending on the Reynolds number laminar, transitional, and turbulent flow behaviour is assumed. Laminar flow assumption yields a huge separation bubble which tends to become unstable. Further, only for the lowest Reynolds number it is possible to obtain a laminar fore body solution combined with turbulent flow at the flaps. For all other Reynolds number conditions the separation in front of the hinge line is so strong that the solution becomes unstable, yielding to unreliable flow solutions for the flaps. Computed solutions for fully turbulent flows show higher levels of heat fluxes but lower gradients than the experimental results.

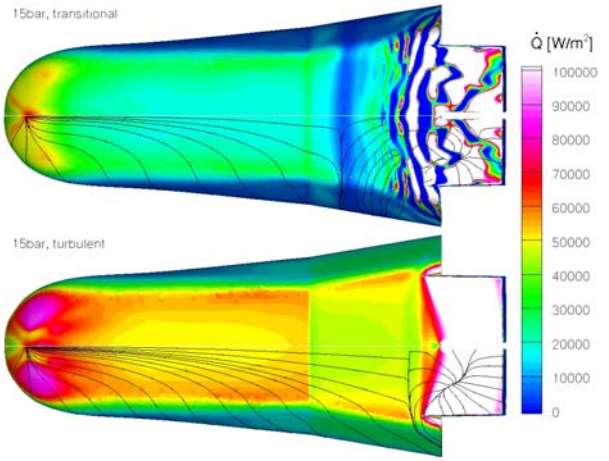

Figure 11: Computed transitional and turbulent heat flux density with skin friction lines for RFMEX in HLB 15bar condition

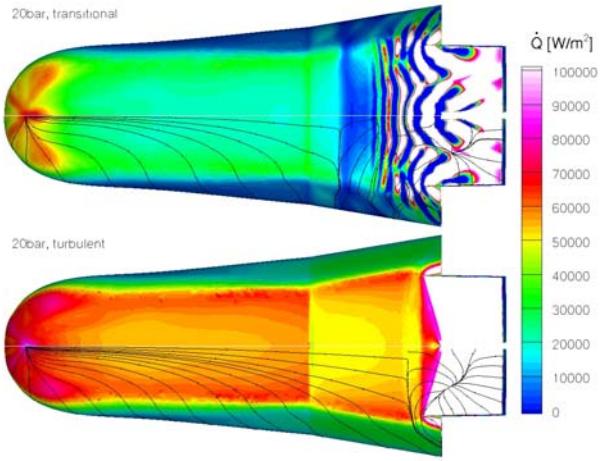

F*igure 12: Computed transitional and turbulent heat flux density with skin friction lines for RFMEX in HLB 20bar condition*

5. CONCLUSIONS

The paper presents an experimental and numerical investigation of the unsteady, transitional flow over at a cantilever flap configuration of a space vehicle in cold hypersonics. The goal of the study is to investigate the potential to use an aerodynamically controlled vehicle to perform an aerobraking manoeuvre when returning from a Moon mission. As the result of a feasibility study comprising a super orbital velocity Earth re-entry at velocities over 11 km/s and recovery manoeuvre with an actively aerodynamic controlled vehicle, the lifting body class was selected as the best option. Two body flaps which are the main components of the aerodynamic control system are attached to the rear of the vehicle in a cantilevered configuration. They are used for vehicle trimming and altitude control.

A preliminary experimental investigation was carried out in the high-speed Ludwig tube facility of the University of Braunschweig, at a Mach 6, Reynolds numbers varying from 2.4 10^6 to 1.7 10^7. All results are obtained for a constant angle of attack of 45deg and 20deg flap deflection angle. By using a Plexiglas model, a high-speed infrared system and a high speed Schlieren camera, infrared mapping and heat transfer rates of the complete surface of the vehicle and flow field visualizations were obtained. In support of the experimental study, numerical solutions were obtained by means of the TAU code of the DLR. Due to the strong complexity of the flow problem a previous exercise to select the most reliable turbulence models is reviewed using generic shapes. Such exercise reflects that only few of the existing turbulence models provide reasonable answers in hypersonic.

The analysis of the experimental and numerical results displays a complex unsteady flow topology at the control surfaces, with severe hot points resulting from shock-shock interaction, shock-boundary layer interaction and jet flow in the gap between the flaps. The resulting jet impingement at the flaps results in heat fluxes which largely surpass the stagnation point heat flux. Such situation becomes more severe as the flow evolves from almost laminar for the low Reynolds number case to transitional at the flaps for the high Reynolds number case. It turns out aerobraking maneuvers with aerodynamic controlled vehicles should be carefully designed as larger body-flap deflections and larger flight Reynolds numbers change the control-surface system of shocks from Edney-Type VI to Type V. The shock system turns out highly unstable, jumping suddenly upstream, and leading to a hysterese motion associated with a massive flow separation on the windward side of the vehicle and hence jeopardizing the whole mission.

While the data put in evidence the weakness associated with excperimental and numerical prediction methods, they shows once more the great potential that coordinated numerical and experimental work can have in the understanding of extremely complex flow topologies. Further, with the present study non-intrusive measurement techniques (optical techniques) have shown their huge potential to capture major features of such complicate flows. Finally, from the numerical point of view such flows should be computed in the future only as unsteady while laminar-turbulent transition continues to be a modelling issue.

6. REFERENCES

[1] Bozic, O.; Longo, J.: Moon Sample Return Mission 2016. Proceedings of the 58th International Astronautical Congress, Hyderabad, India, paper IAC-07-A3.6.B.055th (2007).

[2] Longo, J.; Turner, J.; Weihs, H.: The aerodynamic re-entry controlled Sharp Edge Flight Experiment of DLR. 6th European Symposium on Aerothermodynamics for space vehicles (2008).

[3] Estorf, M.; Wolf, T.; Radespiel, R.: Experimental and numerical Investigations on the operation of the Hypersonic Ludwieg Tube Braunschweig. 5th European Symposium on Aerothermodynamics for space vehicles (2004).

[4] Estorf, M.: Ortsaufgelöste Bestimmung instationärer Wärmestromdichten in der Aerothermodynamik, ZLR-Forschungsbericht 2008-03, Shaker Verlag, Aachen (2008).

[5] Wolf, T.; Estorf, M.; Radespiel, R.: Investigation of the starting process in a Ludwieg tube. Theoretical and computational Fluid Dynamics, Vol. 21, (2007), pp. 81-98.

[6] Lohrengel, J.; Todtenhaupt, R.: Wärmeleitfähigkeit, Gesamtemissionsgrad, und spektrale Emissionsgrade der Beschichtung Nextel Velvet Coating 811-21 (RAL 900 15 tiefschwarz matt). PTB-Mitteilungen, 106 No. 4, (1996), pp. 259-265.

[7] Schwamborn, D., Gerhold, T., Heinrich, R.: The DLR TAU-Code: Recent Applications in Research and Industry. ECCOMAS CFD 2006, TU Delft, The Netherlands (2006).

[8] Schwane, R.: Description of the Testcase: MSTP Workshop 1996 Reentry Aerothermodynamics and Ground-to-Flight Extrapolation. Technical Report YPA/1889, ESTEC, Noordwijk (1996).